The Identification of Multiple Crystalline Zinc Soap Structures Using Infrared Spectroscopy

Hermans, J.; Helwig, K.

DOI
10.1177/0003702820935183

Publication date
2020

Document Version
Final published version

Published in
Applied Spectroscopy

Article

Applied Spectroscopy

Applied Spectroscopy
2020, Vol. 74(12) 1505–1514

DOI: 10.1177/0003702820935183
journals.sagepub.com/home/asp

The Identification of Multiple Crystalline Zinc Soap Structures Using Infrared Spectroscopy

Joen Hermans[1,2] and Kate Helwig[3]

Abstract

The formation of crystalline zinc soaps (zinc salts of fatty acids) in oil paint layers is a common sign of paint degradation. In this study, we have used infrared spectroscopy to systematically identify differences in structure and composition of crystalline zinc soap phases, and report data analysis methods for structure attribution in challenging oil paint samples. Supported by reported crystal structures, it was possible to distinguish two distinct types of zinc soap geometry: a highly symmetrical packing for long-chain saturated soaps (type B) and an alternating packing for zinc soaps with short, unsaturated, or dicarboxylic chains (type A). These two types of packing can be identified by a single or split asymmetric COO stretch vibration band. With this new information, we studied the structure and composition of zinc soaps formed in a zinc white model paint and in a cross-section from the painting *Equations in Space* by Lawren Harris. Using non-negative matrix factorization, band integration and band position maps, it was possible to clearly identify zinc azelate in the model paint and map its spatial distribution. The same methods showed that the paint cross-section contained both types of zinc soap structure within the same paint layer, with the less symmetrical structure appearing only at the interface with the ground layer. The results give valuable information on the internal chemistry of oil paint layers, and the demonstrated methods can find widespread application for in-depth analysis of infrared microscopy data.

Keywords

Zinc soaps, infrared spectroscopy, attenuated total reflection Fourier transform infrared, ATR FT-IR microscopy, oil paint, spectral processing

Date received: 5 February 2020; accepted: 8 May 2020

Introduction

Zinc complexes of fatty acids are a class of compounds with interesting structural properties. These so-called zinc soaps find application as fillers/plasticizers in polymers,[1–4] as stabilizers in polyvinyl chloride (PVC),[5] and as precursors for nanoparticle synthesis.[6,7] However, in the last decade, zinc soaps have also been studied extensively[8–14] as a degradation product in oil paintings that contain zinc white (ZnO) pigment, one of the most common white pigments used by artists in the late 19th and 20th centuries.[15] Forming as a result of chemical reactions that break down the ZnO pigment and the oil binder,[16] zinc soaps have been associated with many undesirable changes in the appearance and structural integrity of oil paintings, including increased paint transparency and delamination of paint layers.[17] As part of ongoing research to investigate the reaction pathways that lead to paint degradation[18] and possible strategies to minimize future changes,[19] it is important to have the ability to distinguish between different crystalline zinc soap phases and to identify the specific fatty acids involved in zinc soap crystallization. In a typical drying oil used for oil paint, both carboxylic acids with saturated and unsaturated alkyl chains can be present, having one or two carboxylic acid end-groups.[20]

Fourier transform infrared (FT-IR) spectroscopy and microscopy have proven to be very practical techniques to detect zinc soaps in a polymer matrix and to study their molecular structure. The series of progression bands in the infrared (IR) spectrum, caused by coupled CH_2 vibrations in all-*trans* methylene chains, is

[1]Van 't Hoff Institute for Molecular Sciences, University of Amsterdam, Amsterdam, The Netherlands
[2]Conservation & Science, Rijksmuseum, Amsterdam, The Netherlands
[3]Canadian Conservation Institute, Ottawa, Canada

Corresponding Author:
Joen Hermans, Van 't Hoff Institute for Molecular Sciences, University of Amsterdam, PO Box 94157, 1090GD Amsterdam, The Netherlands
Email: j.j.hermans@uva.nl

characteristic of the length of the hydrocarbon chain of the fatty acid molecules.[21] Furthermore, the strong asymmetric stretch vibration of the carboxylate group (ν_a COO) is particularly sensitive to subtle changes in coordination geometry. Recently, this useful feature in IR spectra of zinc carboxylates was successfully employed to resolve the water-sensitive structures of non-crystalline zinc soap complexes.[22] For crystalline zinc soaps, however, some ambiguity remains. While the ν_a COO vibration shows a single band around 1538 cm^{-1} for zinc soaps of long-chain saturated fatty acids, the band has been described as a doublet for zinc soaps with unsaturated chains,[9,10] suggesting that there are at least two different coordination geometries possible. In oil paint samples, both the single and the double band types are regularly detected,[9,13,23] but a clear interpretation of these spectral differences in terms of crystal structure and fatty acid type has so far remained challenging.

In this paper, we use attenuated total reflection FT-IR spectroscopy (ATR FT-IR) in combination with reported reference crystal structures to definitively match IR spectral features to coordination geometries and fatty acid types for crystalline zinc soaps. Moreover, we demonstrate the usefulness of non-negative matrix factorization (NMF) and data visualizations other than band integral maps for the interpretation of FT-IR microscopy data and the distinction between chemical species in model and real paint samples.

Experimental

Preparation of Materials

Zinc soap reference materials (zinc caproate, caprylate, caprate, laurate, myristate, palmitate, stearate, azelate, and oleate) were synthesized by precipitation from an alkaline solution of zinc nitrate and fatty acid, as previously described.[24] All materials were thoroughly dried prior to analysis.

The zinc oxide model paint film was prepared by grinding ZnO (Sigma-Aldrich, nano-powder <100 nm) together with linseed oil (Kremer, untreated cold-pressed) in a 1:1 weight ratio. The paint mixture was spread on a glass slide with a draw-down bar to a wet thickness of 60 μm, after which the slide was placed in a sealed container at 60 °C for 38 days with a water reservoir to achieve 99% relative humidity (RH). These ageing conditions were chosen to promote extensive oil network oxidation and hydrolysis, and ultimately the formation of zinc soaps. The paint film was extremely brittle and difficult to handle after ageing.

A paint cross-section sample from the painting *Equations in Space* was mounted in polyester resin, and subsequently ground and polished using standard petrographic techniques. An additional sample was taken of a waxy zinc soap protrusion for transmission FT-IR spectroscopy.

Analytical Methods

ATR FT-IR spectra of bulk samples were collected on a Frontier spectrometer (Perkin-Elmer) equipped with a heatable diamond GladiATR module (Pike Technologies). Spectra were collected with four scans and 4 cm^{-1} resolution. ATR FT-IR microscopy experiments were carried out on a Spotlight 400 system (Perkin-Elmer) equipped with a 16-pixel mercury cadmium telluride (MCT) array detector and a germanium crystal ATR sample holder (600 μm diameter footprint). These spectra were also averaged over four scans and acquired at 4 cm^{-1} spectral resolution. While the maps were acquired at a pixel step size of 1.56 μm, the achieved spatial resolution, which is dependent on many other optical factors,[25,26] was not determined in this study. The isolated paint protrusion was mounted in a low-pressure diamond anvil microsample cell and analyzed using a Hyperion 2000 microscope (Bruker) with an MCT detector interfaced to a Tensor 27 spectrometer. The sample was measured in transmission mode by co-adding 200 scans and using a 4 cm^{-1} resolution.

Powder X-ray diffraction (XRD) analysis was carried out with a Miniflex II desktop X-ray diffractometer (Rigaku) with Cu Kα radiation ($\lambda = 1.54180$ Å) at 30 kV and 15 mA. Diffractograms were recorded in a $2\theta = 1$–40° range (5°/min scan rate and 0.05° step size). Contribution of the Cu Kα2 line was subtracted before analysis. Samples were prepared by manually pressing finely ground powder in a glass sample holder.

Data Analysis

For ATR FT-IR spectra of bulk samples, baseline correction, normalization, and integration were carried out with custom scripts written in Wolfram Mathematica software. These scripts are available from the authors upon reasonable request. The spectra were shifted by subtracting the lowest absorbance value in the spectrum and normalized on the total area of the ν_a COO bands (integration between 1480 and 1600 cm^{-1}).

All FT-IR microscopy data were analyzed using the ROI Imaging tool of the free and open-source PyMCA software package (v. 5.5.4).[27] While originally written for analysis of X-ray fluorescence data, the software provides many tools for correction, integration, visualization, and statistical analysis of datacubes of any sort.

For band integration maps, a statistics-sensitive nonlinear iterative peak-clipping (SNIP) background was subtracted to account for baseline shifts, considering only the 750–1800 cm^{-1} spectral range and using a width of 60 cm^{-1}.

For NMF, a gradient descent constrained least-squares algorithm was used, and the data were limited to the ranges 750–1800 cm^{-1} and 2800–3050 cm^{-1} to minimize the influence of parts of the spectra that carry little information, unless noted otherwise. Briefly, the NMF algorithm approximates the original dataset by a multiplication of two positive matrices: one containing a chosen small number of base

spectra, the other listing for each pixel the weight factors required in a linear combination of the base spectra to approximate the original data in that pixel. Ideally, these base spectra or *components* match the spectrum of a pure compound in the sample. In practice, however, the concentrations of compounds within a sample are rarely completely independent, so an NMF component may contain contributions of one or more (partially) correlated pure compounds. Moreover, most NMF algorithms are initialized with a random component matrix, which means that multiple local minimum solutions may be found for different runs of the algorithm. Nevertheless, for IR datasets with considerable spectral variation, NMF can give fast and reliable insight in the spatial distribution of species, even when spectra are strongly congested. In this work, NMF runs were repeated at least 10 times to verify the robustness of the NMF weight factor map and the results of the components.

All conclusions based on ATR FT-IR microscopy data were cross-checked by comparing large numbers of spectra from different regions in each map. More detailed information on the stepwise application of PyMCA tools for the analyses described in this paper is available from the authors upon reasonable request.

Results and Discussion

Infrared Spectra of Pure Zinc Soaps

To make a link between the crystal structures of zinc soaps and their spectral features, we started by investigating a series of ATR FT-IR spectra of synthesized zinc soaps. Figure 1 shows the FT-IR spectra of zinc oleate (*cis*-octadecenoate), zinc azelate (nonanedioic acid), and a series of saturated zinc soaps with chain lengths increasing from 6 to 18 carbons. Oleic, azelaic, palmitic, and stearic acid are all routinely found in aged oil paint binders.[20] The positions of the main characteristic bands are listed in Table S1, Supplemental Material.

Within the series of zinc soaps with monocarboxylic saturated chains, from caproate to stearate, a transition in structure can be observed between C8 and C10. While there is slight variation in the exact band positions, the zinc soaps with short alkyl chains all show at least three asymmetric carboxylate stretch vibration bands around 1527, 1547, and 1592 cm^{-1}, possibly with a fourth band around 1500 cm^{-1}. The long-chain zinc soaps show only one ν_a COO band around 1537 cm^{-1}. The symmetric COO stretch vibration around 1400 cm^{-1} shows a similar transition from split to single bands. The transition in this zinc soap series suggests that the crystal structure in the long-chain zinc soaps is more symmetric than the short-chain soaps. As a consequence of increasing alkyl chain length, there are also clear increasing trends in the total intensity of the CH_2 and CH_3 stretch vibrations (see Figure S1, Supplemental Material), the relative intensities of the CH_2 bands (2846 and 2915 cm^{-1}) and the CH_3 bands (2866 and 2950 cm^{-1}), and the number of progression bands in the region 1180–1380 cm^{-1} caused by coupled CH_2 vibrations in all-*trans* methylene chains.[21] Interestingly, the IR spectra of zinc oleate (C18:1) and

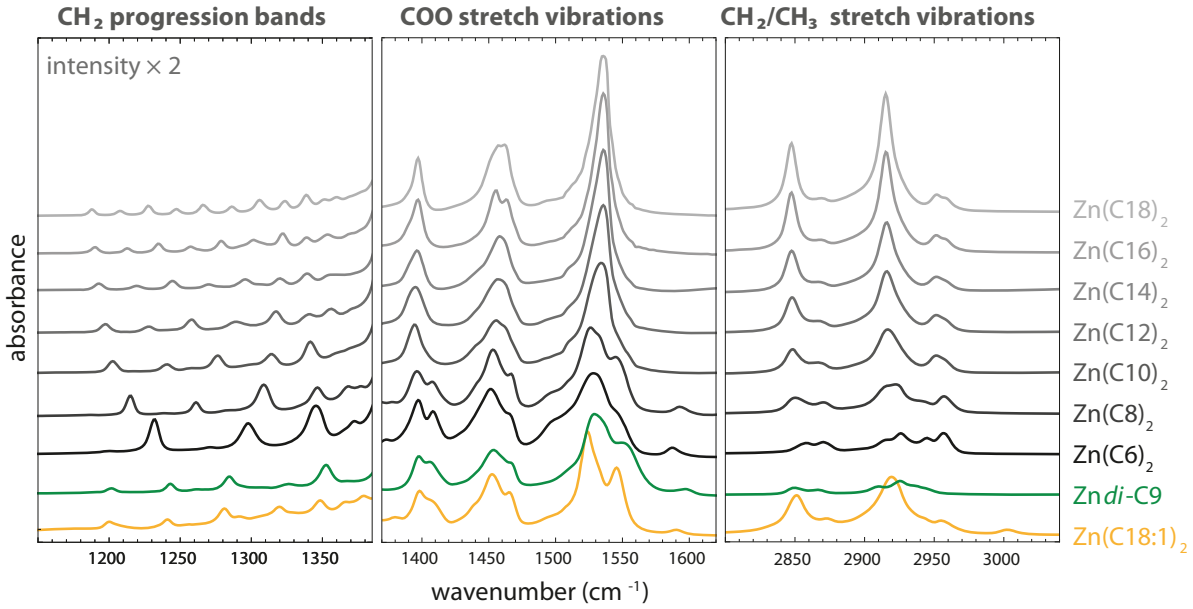

Figure 1. ATR FT-IR spectra of zinc soap complexes with oleate (C18:1) and azelate (*di*-C9) chains, and a series with saturated alkyl chains increasing from six to 18 carbon atoms long. All spectra were baseline-corrected, normalized on the total area of the ν_a COO bands (integration between 1480 and 1600 cm^{-1}), and shifted vertically for clarity. A table with the positions of all relevant bands can be found in the Supplemental Material.

zinc azelate (*di*-C9) also show a split carboxylate band structure, similar to the short-chain zinc soaps.

Reference Zinc Soap Structures

The distinction between two types of zinc soap crystal structure is supported by XRD studies reported in the literature. Lacouture et al. carried out single-crystal XRD on zinc octanoate,[28] which adopts the structure typical for metal soaps where sheets of coordinated zinc ions are separated by extended alkyl chains (Figs. 2a to 2c). In this zinc soap structure of type A, each zinc ion is tetrahedrally coordinated by oxygen atoms from four different carboxylate groups. Figures 2b and 2c show clearly that each consecutive layer in the plane of Fig. 2b is rotated by 180°, resulting in crossed alkyl chains. This rotation means that the ZnO_4 tetrahedra in the zinc sheet are alternating in orientation moving down the plane of Fig. 2b and that the transition dipole moments of the ν_a COO vibrations (pointing from one carboxylate oxygen to the other) are not aligned. In turn, this lack of alignment gives rise to multiple bands corresponding to in-phase and out-of-phase vibrational modes. Despite the presence of two carboxylate headgroups per alkyl chain in azelaic acid, the crystal structure of zinc azelate reported by Tamames-Tabar et al. contains sheets of ZnO_4 tetrahedra with the same alternating orientation as zinc octanoate,[29] which explains the similarity of their FT-IR spectra.

In contrast, the structure reported by Mesbah et al.[30] of zinc dodecanoate, based on Rietveld refinement of powder XRD data, is more symmetric (Figs. 2d to 2f). In this structure of type B, the chains on either side of the zinc sheet are different only by rotation. Moreover, all chains on the same side of the zinc sheet are identically oriented, which means that all ZnO_4 tetrahedra also have identical orientation. This high degree of symmetry explains why the FT-IR spectrum of zinc soaps with this geometry shows a single ν_a COO band: on both sides of the zinc sheet all carboxylate transition dipole moments are aligned to give rise to one strong in-phase vibration and both sides of the zinc sheet

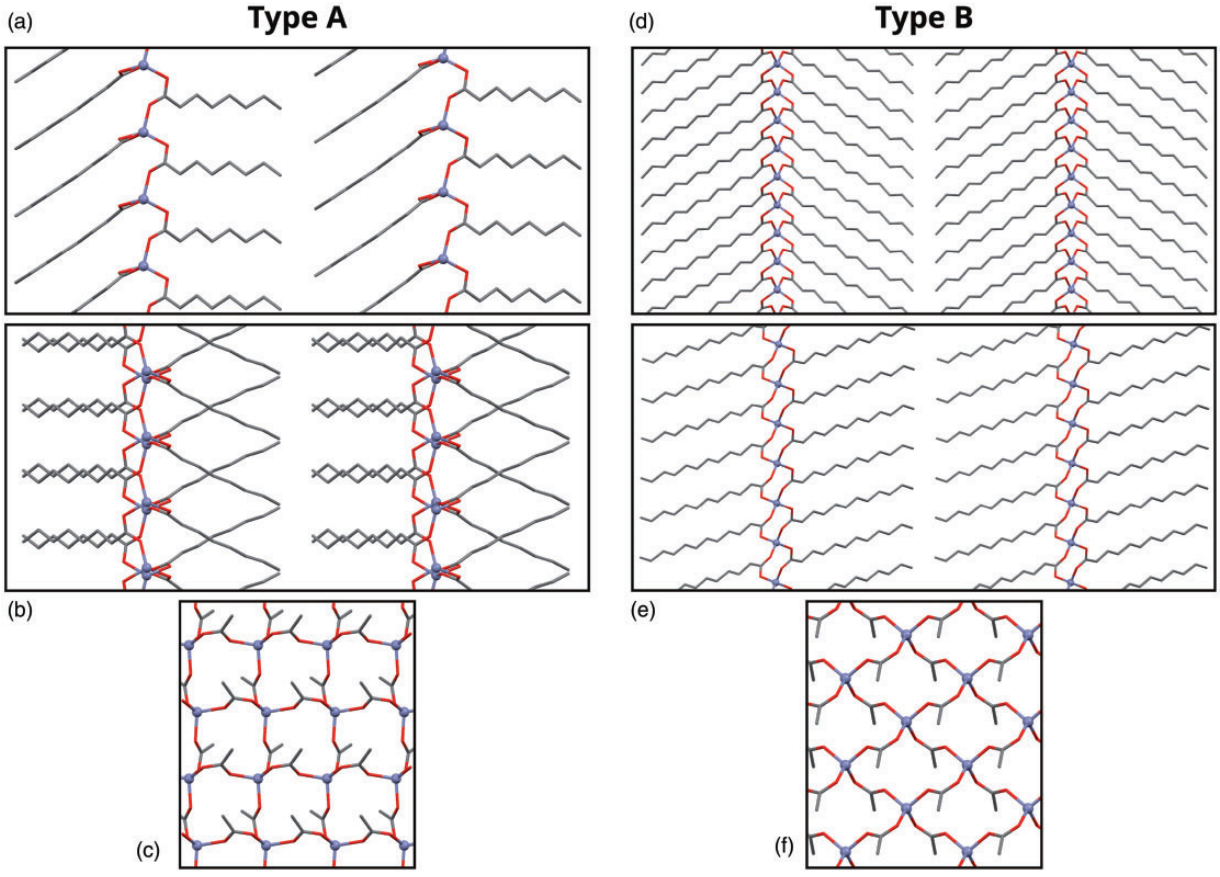

Figure 2. A comparison of crystal structure along the three axes of the unit cell of the two types of zinc soap geometry, one favored by zinc carboxylate coordination (a–c, type A) and one governed by Van der Waals interactions of the alkyl chains (d–f, type B). Zinc ions are indicated as blue spheres, oxygen is red, and carbon is gray. Hydrogens are omitted, and in (c,f) only the first carbon atom in the chain is depicted, for clarity. Images are based on the single-crystal XRD structure of zinc octanoate[28] and the crystal structure derived from powder XRD data of zinc dodecanoate.[30]

are structurally identical. Interestingly, the transition from type A to type B structure causes only a very small difference in the spacing between the zinc sheets,[24,31] which is an easily measured metric derived from the series of long spacing peaks in powder XRD experiments that is often used to characterize metal soaps.

Powder XRD analysis of the zinc soap samples corresponding to the FT-IR spectra shown in Fig. 1 confirmed that these zinc soaps match the reported type A and type B crystal structures (Figure S2, Supplemental Material).

The most likely explanation for the existence of two types of crystalline zinc soaps lies in the balance between optimizing the coordination geometry around the zinc ions and maximizing the Van der Waals interactions of the alkyl chains. For short alkyl chains, zinc carboxylate coordination dominates and a structure of type A geometry is the optimal, lowest energy configuration. Type B geometry has non-ideal zinc coordination and only occurs when zinc soap structure is dominated by the interaction between the alkyl chains. As the alkyl chain length increases, the zinc soap structure can be optimized by switching from square to hexagonal alkyl chain packing (Figure S3, Supplemental Material), leading to the chain-dominated type B structure. At intermediate chain length, the energy difference between type A and type B structures is so small that both types seem to co-exist, as reported by Mesbah and François for C11 chains.[31] This transition from optimal coordination to optimal chain packing is highly similar to the structural transition reported for lead soaps,[32,33] where the lead ions switch from hemidirected to holodirected coordination around an alkyl chain length of nine carbons.

In conclusion, whenever the alkyl chains in zinc soaps have the potential for a large gain in Van der Waals interaction energy, the symmetric packing type B is adopted. When this gain is not possible because the alkyl chains are short, the asymmetric packing of type A with optimized zinc coordination is favored. The spectroscopic evidence

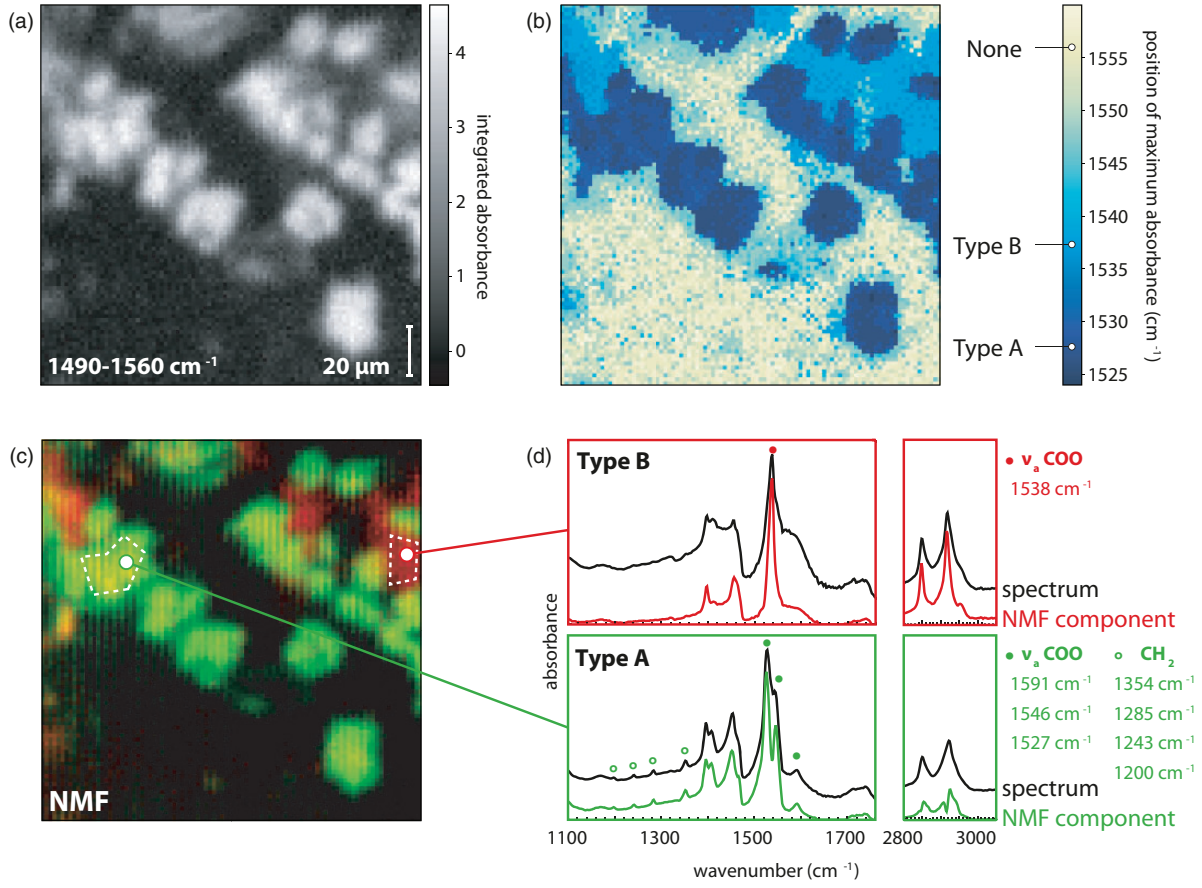

Figure 3. Illustration of various methods for the analysis of IR microscopy data. (a) Map of integrated absorbance in the range 1490–1560 cm^{-1}, after subtraction of the area under a straight line between the limits of the wavenumber range. (b) Map of the position of maximum intensity in the range 1524–1560 cm^{-1}. (c) Map of two NMF weight factors corresponding to the NMF components in (d). (d) Comparison between two NMF components and averaged IR spectra from two dashed line regions indicated in (c). The IR spectra were shifted vertically for clarity.

suggests that zinc oleate also adopts type A zinc carboxylate coordination, probably because the *cis* double bond in oleic acid complicates neat packing of the chains. In light of this, perhaps type A coordination can also occur with long-chain saturated fatty acids if the zinc soaps are forming inside a densely cross-linked polymer matrix such as aged oil paint. When metal soap crystallization occurs in such a matrix, molecular movement may be restricted, which might lower the degree of order in alkyl chain packing and thereby cause type A zinc carboxylate coordination. In support of this idea, transmission electron microscopy experiments have shown that zinc soap material formed in ZnO model paint is indeed very irregular, with crystalline domain sizes in the order of tens of nanometers.[12] Moreover, FT-IR spectra of zinc palmitate recrystallized from linseed oil have been reported that showed some signs of ν_a COO band splitting.[34]

Identification of Zinc Soaps in a Model Oil Paint

Understanding the relation between zinc soap structures and their FT-IR spectra allows us to investigate the structure of zinc soaps formed in a model oil paint sample. A $150 \times 150\,\mu m$ map of FT-IR spectra was acquired on the top surface of a strongly aged film of ZnO pigment in linseed oil using ATR FT-IR microscopy.

Several strategies for the analysis of IR microscopy data are illustrated in Fig. 3 to establish the identity of the crystalline zinc soaps formed in the paint. Figure 3a shows a map of integrated absorbance in the range of the ν_a COO band of zinc soaps (1490–1560 cm^{-1}) after baseline subtraction. The map clearly shows a number of regions that contain a high concentration of crystalline zinc soaps. However, because of the large extent of overlap of the ν_a COO bands of type A and type B zinc soap structures, it is challenging to map possible differences in structure by band integration. Interestingly, such a distinction can be visualized easily when we consider the differences in position of the most intense ν_a COO bands for type A and type B zinc soap structures (1525–1530 and 1535–1538 cm^{-1}, respectively). In Fig. 3b, the colors indicate the wavenumber at which maximum absorbance is measured within the range 1524–1560 cm^{-1}. This map yields a clear view on the dominant band within a certain wavenumber range. In this case, we see that most of the areas with high integrated absorbance in Fig. 3a correspond to zinc soaps of type A, while some regions with lower intensity signal in between those areas are dominated by zinc soaps of type B. Since the type B structure can only be formed with long-chain saturated fatty acids, we can conclude that a relatively minor fraction of the total crystalline zinc soap concentration within this region of the sample corresponds to zinc stearate and zinc palmitate or their mixtures.[9]

To investigate the identity of the crystalline zinc soaps in more detail, we applied NMF to the IR datacube. Figure 3c shows an NMF map with the distribution of two distinct zinc soap species. Whereas the band position map (Fig. 3b) shows only where, if any, both types of zinc soap structure are *dominant*, the NMF map is directly correlated to the concentration of each species. The NMF components associated to the map are shown in Fig. 3d, along with averaged IR spectra from two regions rich in either species. By comparing the NMF components and the averaged IR spectra, it is immediately obvious that the green and red regions in the NMF map correspond to the zinc soap structures of type A and type B, confirming the conclusion of the band position map. It is interesting to note that the NMF components contain less contribution of other species in the sample, such as the ester band at 1740 cm^{-1} from the oil polymer and the broad non-crystalline zinc carboxylate band[22] centered around 1600 cm^{-1}. Because the NMF components are relatively pure, in this case it is easier to analyze the splitting of the ν_a COO band and the relative intensities of other bands with NMF components than with extracted FT-IR spectra.

The spectra of type A show interesting details that allow us to identify not only the coordination geometry but also the identity of the fatty acid in the zinc soap. The CH_2 stretch vibrations in the type A spectra seem to be much less intense than those in the type B spectra, which suggests that the alkyl chain in these type A zinc soaps is shorter. Moreover, we can distinguish a clear set of CH_2 progression bands at 1354, 1285, 1243, and 1200 cm^{-1}, which match very well only with those observed for zinc azelate (Figure 1 and Table S1, Supplemental Material). To completely exclude the possibility that these type A zinc soaps are long-chain zinc soaps with only a short section of their alkyl chains neatly packed and extended, a different sample of the paint film was heated to 150°C while recording ATR FT-IR spectra (Figure S4, Supplemental Material). At this temperature, which is between the melting point of zinc stearate (131 °C)[34] and the melting/decomposition temperature of zinc azelate (>300 °C),[35] the FT-IR spectrum still showed the split ν_a COO band of type A zinc soaps, proving that a large fraction of the zinc soaps formed in this sample is zinc azelate. The detection of such a high concentration of azelaic acid salts supports previous observations that ageing under high-humidity/temperature conditions promotes oxidation and chain scission of the unsaturated fatty acid chains in drying oils.[20,36]

Identification of Zinc Soaps in a Cross-Section Sample from an Oil Painting

The painting *Equations in Space* by Lawren Harris (1936, National Gallery of Canada) exhibits cracking and lifting paint as well as disfiguring zinc soap protrusions at the surface. The source of the zinc soaps responsible for the cracking and lifting are the lowest paint layers of the composition.[9,13]

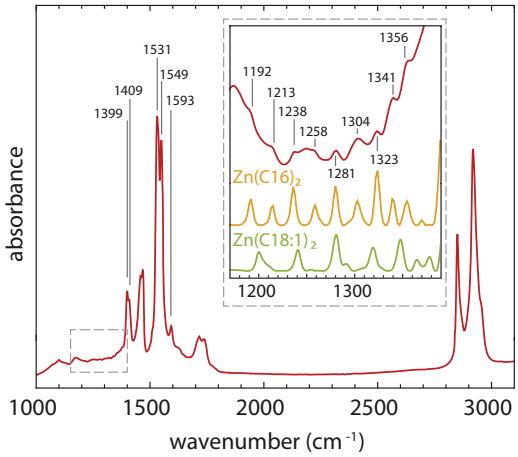

Figure 4. FT-IR transmission spectrum of an isolated paint protrusion that was composed mostly of type A crystalline zinc soaps. The inset is a magnification showing a comparison between the weak series of CH_2 progression bands in the spectrum of the isolated protrusion and the baseline-corrected progression bands of zinc palmitate and zinc oleate.

Figure 4 shows the transmission FT-IR spectrum of an isolated paint protrusion composed mostly of zinc soaps. The spectrum shows clear features of a type A zinc soap structure with ν_a COO band maxima at 1531, 1549, and 1593 cm^{-1}. There is no C=C–H stretch vibration band visible around 3005 cm^{-1}, which rules out the presence of a substantial amount of zinc oleate or other unsaturated fatty acids. Moreover, there is a clear set of CH_2 progression bands which match very well with those of zinc palmitate (see Table S1, Supplemental Material), with a likely minor contribution of stearate. Indeed, gas chromatography–mass spectrometry (GC-MS) measurements carried out previously confirm that palmitate and stearate are the main fatty acids present in the zinc soap sample, with only a minor concentration of azelate and oleate.[9] Based on the CH_2 progression bands and GC-MS results, we conclude that the zinc soaps in this isolated sample are zinc soaps of long-chain saturated fatty acids that have (partially) crystallized in a type A geometry, even though it is not their most stable form.

To investigate the formation of these type A zinc soaps in more detail, we measured a cross-section sample from the painting with ATR FT-IR microscopy. Compared to model oil paints, samples from real paintings are usually more challenging to analyze. Typically, multiple paint layers are present, each containing several pigments, additives, and/or fillers. Additionally, the volume of sample material from valuable artworks is obviously limited. The paint sample was embedded in a polymerized resin block, after which polishing revealed the stratigraphy of the painting.

Figure 5a shows a visible light microscopy image of a cross-section taken next to a loss (Fig. 5a). NMF analysis of an ATR FT-IR microscopy dataset collected on that sample allowed easy distinction among three blue layers and showed that the zinc soaps were concentrated in the lowest blue layer (Fig. 5b). Selected ranges of the corresponding NMF components show clear features consistent with lead carbonate in the top layer (1390 cm^{-1}), lead sulfate in the middle layer (1045 cm^{-1}), and crystalline zinc soaps in the bottom layer (1536 cm^{-1}). However, it proved very difficult to make a distinction between different zinc soap structures within the bottom layer with NMF. Restricting the data to a section of the bottom paint layer, thereby reducing the number of individual chemical species within the dataset did not result in a clear distinction between type A and type B zinc soap structures.

The map of integrated ν_a COO band intensity shows that there is a gradient in the concentration of crystalline zinc soaps in the sample (Fig. 5c). While there are zinc soaps present in the entire lower blue layer, the concentration is highest in a thin band along the lower edge where it is in contact with the ground layer. Looking at the position of the ν_a COO band in this paint layer (Fig. 5d), we can see a stark contrast between the bottom edge of the paint layer, dominated by type A zinc soaps, and the bulk of the layer, containing more zinc soaps of type B. This clear distinction is confirmed by looking at averaged spectra from the two regions indicated in Fig. 5a. Region 1 shows a split ν_a COO band of type A (Fig. 5e), while region 2 shows a single type B band (Fig. 5f). The significance of the type A split COO band feature was confirmed by comparing 10 randomly selected spectra from region 1 with their average, which showed that the split band clearly persists after averaging while the overall noise level was greatly reduced (Figure S5, Supplemental Material). Interestingly, with the knowledge that both zinc soap types are present within this sample, we succeeded in tweaking the analysis parameters to visualize the same result both with a band integration map and with NMF (see Figure S6, Supplemental Material).

Due to a lack of discernible CH_2 progression bands in the spectra in Figs. 5e and 5f, it is not possible to identify the fatty acid composition of the type A zinc soaps at the bottom edge of the blue paint layer with certainty. However, we consider it unlikely that these zinc soaps have a very different fatty acid composition than the isolated zinc soap protrusion sample, which contained only minor fractions of oleate and azelate. Therefore, we hypothesize that zinc soaps of long-chain saturated fatty acids have adopted a type A coordination geometry along the bottom edge of the blue paint layer.

There are many possible explanations for this interesting finding. The FT-IR spectra in Figs. 5e and 5f show that the ester carbonyl stretch vibration band is much more intense along the bottom edge than in the bulk of the paint layer. Other FT-IR bands typical for the polymerized oil binder were also more intense along the bottom edge. This observation could mean that during drying and ageing, there has been migration of oil medium in the blue paint layer to the

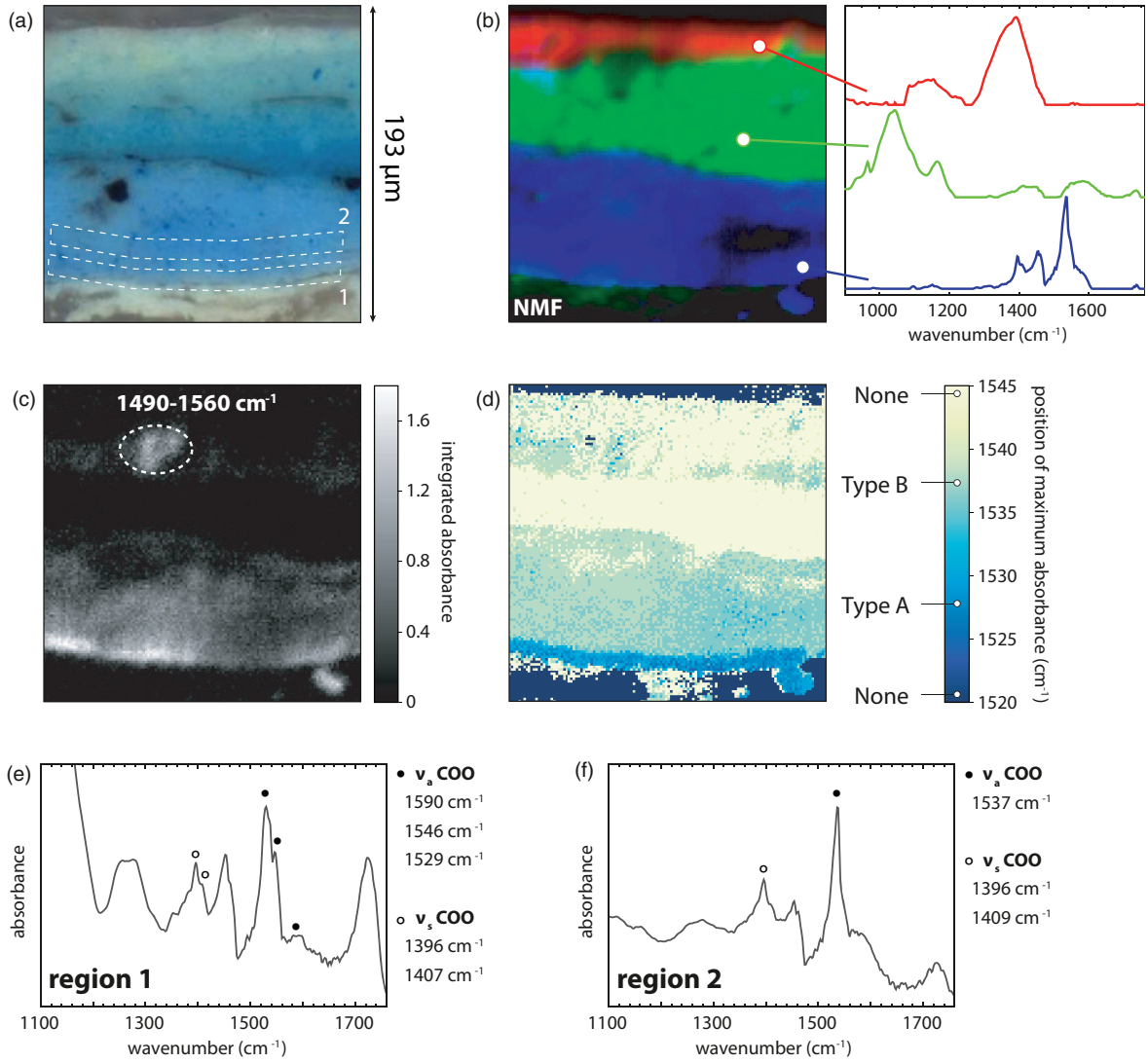

Figure 5. (a) Optical microscopy image of a paint sample from *Equations in Space* by Lawren Harris (1936, National Gallery of Canada). This cross-section shows four blue paint layers and fragments of a white ground layer at the bottom where delamination has taken place. Dashed lines indicate the regions averaged to yield the spectra in (e) and (f). (b) NMF map showing the weight factors corresponding to three components dominant in each paint layer. (c) Map of integrated absorbance in the range 1490–1560 cm^{-1}, after subtraction of the area under a straight line between the limits of the wavenumber range. The signal in the dashed oval is caused by contamination with proteinaceous material. (d) Map of the position of maximum intensity in the range 1520–1545 cm^{-1}. (e, f) Averaged spectra corresponding to the regions indicated in (a).

lower interface where it is in contact with the lean, crumbly ground. In addition, it could be that the binding medium along the bottom edge is less hydrolyzed and thus less fragmented than the bulk. Both a higher binder concentration and a more intact polymer network near the interface may hinder chain alignment in the zinc soap crystals, producing type A coordination, while the zinc soaps in the bulk of the paint layer crystallized in the preferred type B coordination.

Alternatively, the formation of type A or B crystalline geometries could be related to the crystallization rate. If the type A structure is a metastable polymorph of the lowest-energy type B geometry for zinc soaps of long-chain saturated fatty acids, one would expect slower crystal growth rates to cause formation of stable type B zinc soaps, while rapid crystallization could lead to the appearance of the metastable type A intermediate.

The presence of gradients in polymerization degree or binder concentration and their potential effects on zinc soap crystallization rate remain unclear at this moment. Careful study of a wider range of paint samples and model systems with the techniques described above could help to answer these questions, and is currently underway.

Conclusion

The study of ATR FT-IR spectra of a range of zinc soaps and comparison with known crystal structures has allowed the distinction between two geometry types for crystalline zinc soaps. The splitting of the asymmetric COO stretch vibration band in FT-IR spectra is a key feature that allows distinction between these two types of zinc soap structure. Moreover, careful study of the CH_2 progression bands, the C=C–H stretching band, and the relative intensities of alkyl and carboxylate bands can support a definitive identification of the fatty acids involved in zinc soap formation.

The acquired knowledge was successfully applied to the study of model paint samples and a cross-section sample from a real painting. Using a combination of band integration, NMF analysis and band position maps, clear distinctions could be made between different zinc soaps such as zinc palmitate, zinc azelate, and zinc oleate. In turn, these differences can give interesting information about the local chemical conditions in an artwork. For instance, the detection of zinc azelate indicates that there was extensive oxidation of the binding medium at the time when hydrolysis reactions became significant. The demonstrated methods can find widespread application during routine analysis of samples of oil paints or other materials with FT-IR microscopy.

Acknowledgments

We would like to acknowledge Stephen Gritt (National Gallery of Canada), who noted the degradation issues on *Equations in Space* and brought the protrusions to the authors' attention. The authors also thank Marit Beerse (University of Amsterdam) for preparing the model oil paint sample, and Stephanie Zaleski (Northwestern University) and Maeve Moriarty (Canadian Conservation Institute) for helpful discussions. Lambert Baij, Katrien Keune, and Piet Iedema are acknowledged for ongoing collaborations in zinc soap research.

Declaration of Conflicting Interests

The author(s) declared no potential conflicts of interest with respect to the research, authorship, and/or publication of this article.

Funding

Part of this research was kindly supported by Fonds1999 and the Bennink Foundation/Rijksmuseum Fonds. JH is supported by the Netherlands Organization for Scientific Research (NWO) under project number 016. Veni.192.052.

ORCID iD

Joen Hermans https://orcid.org/0000-0002-9446-9904

Supplemental material

The supplemental material mentioned in the text, consisting of figures and tables, is available in the online version of the journal.

References

1. D.A. Jackson, J.T. Koberstein, R.A. Weiss. "Small-Angle X-ray Scattering Studies of Zinc Stearate-Filled Sulfonated Poly(ethylene-co-propylene-co-ethylidene norbornene) Ionomers". J. Polym. Sci. B. 1999. 37: 3141–3150.
2. P. Antony, S. De. "The Effect of Zinc Stearate on Melt-Processable Ionomeric Blends Based on Zinc Salts of Maleated High-Density Polyethylene and Maleated EPDM Rubber". Polymer. 1999. 40: 1487–1493.
3. R. Dolog, R. Weiss. "Properties and Shape-Memory Behavior of Compounds of a Poly(ethylene-co-methacrylic acid) Ionomer and Zinc Stearate". Polymer. 2017. 128: 128–134.
4. D. Basu, A. Agasty, A. Das, et al. "Phase Changing Stearate Ions as Active Fillers in Multifunctional Carboxylated Acrylonitrile-Butadiene Composite: Exploring the Role of Zinc Stearate". J. Appl. Polym. Sci. 2019. 137(2): 48271.
5. G. Lévai, G. Ocskay, Z. Nyitrai, et al. "Kinetics of the Stabilizing Effect of Calcium and Zinc Stearates in the Thermal Degradation of PVC: Part I". Polym. Degrad. Stabil. 1989. 25: 61–72.
6. S.H. Choi, E.G. Kim, J. Park, et al. "Large-Scale Synthesis of Hexagonal Pyramid-Shaped ZnO Nanocrystals from Thermolysis of Zn-Oleate Complex". J. Phys. Chem. B. 2005. 109(31): 14792–14794.
7. S. Mishra, S. Daniele, L.G. Hubert-Pfalzgraf. "Metal 2-ethylhexanoates and Related Compounds as Useful Precursors in Materials Science". Chem. Soc. Rev. 2007. 36(11): 1770.
8. G. Osmond, J.J. Boon, L. Puskar, et al. "Metal Stearate Distributions in Modern Artists' Oil Paints: Surface and Cross-Sectional Investigation of Reference Paint Films Using Conventional and Synchrotron Infrared Microspectroscopy". Appl. Spectrosc. 2012. 66(10): 1136–1144.
9. K. Helwig, J. Poulin, M.-C. Corbeil, et al. "Conservation Issues in Several Twentieth-Century Canadian Oil Paintings: The Role of Zinc Carboxylate Reaction Products". In: K. van den Berg, editor. Issues in Contemporary Oil Paint. Cham, Switzerland: Springer International Publishing, 2014, pp.167–184.
10. J.J. Hermans, K. Keune, A. van Loon, et al. "An Infrared Spectroscopic Study of the Nature of Zinc Carboxylates in Oil Paintings". J. Anal. Atom. Spectrom. 2015. 30: 1600–1608.
11. F. Gabrieli, F. Rosi, A. Vichi, et al. "Revealing the Nature and Distribution of Metal Carboxylates in Jackson Pollock's Alchemy (1947) by Micro-Attenuated Total Reflection FT-IR Spectroscopic Imaging". Anal. Chem. 2017. 89(2): 1283–1289.
12. J. Hermans, G. Osmond, A.V. Loon, et al. "Electron Microscopy Imaging of Zinc Soaps Nucleation in Oil Paint". Microsc. Microanal. 2018. 24(3): 318–322.
13. E.J. Henderson, K. Helwig, S. Read, et al. "Infrared Chemical Mapping of Degradation Products in Cross Sections from Paintings and Painted Objects". Heritage Science. 2019. 7(71): 1–15.
14. C. Romano, T. Lam, G.A. Newsome, et al. "Characterization of Zinc Carboxylates in an Oil Paint Test Panel". Stud. Conserv. 2020. 65(1): 14–27.
15. G. Osmond. "Zinc White: A Review of Zinc Oxide Pigment Properties and Implications for Stability in Oil-Based Paintings". AICCM Bull. 2012. 33: 20–29.
16. J. Hermans. Metal Soaps in Oil Paint. [PhD Thesis]. Amsterdam: University of Amsterdam, 2017.
17. L. Raven, M. Bisschoff, M. Leeuwestein, et al. "Delamination Due to Zinc Soap Formation in an Oil Painting by Piet Mondrian (1872–1944)". In: F. Casadio, K. Keune, P. Noble, et al, editors. Metal Soaps in Art: Conservation and Research. Cham, Switzerland: Springer International Publishing, 2019, pp.345–357.
18. L. Baij, J.J. Hermans, K. Keune, et al. "Time-Dependent ATR-FTIR Spectroscopic Studies on Fatty Acid Diffusion and the Formation of Metal Soaps in Oil Paint Model Systems". Angew. Chem. 2018. 57: 7351–7354.

19. L. Baij, A. Astefanei, J. Hermans, et al. "Solvent-Mediated Extraction of Fatty Acids in Bilayer Oil Paint Models: A Comparative Analysis of Solvent Application Methods". Heritage Sci. 2019. 7(31): 1–8.
20. F. Modugno, F. Di Gianvincenzo, I. Degano, et al. "On the Influence of Relative Humidity on the Oxidation and Hydrolysis of Fresh and Aged Oil Paints". Sci. Rep. 2019. 9: 5533.
21. S. Barman, S. Vasudevan. "Contrasting Melting Behavior of Zinc Stearate and Zinc Oleate". J. Phys. Chem. B. 2006. 110(2): 651–654.
22. J.J. Hermans, L. Baij, M. Koenis, et al. "2D-IR Spectroscopy for Oil Paint Conservation: Elucidating the Water-Sensitive Structure of Zinc Carboxylate Clusters in Ionomers". Sci. Adv. 2019. 5(6): eaaw3592.
23. G. Osmond. "Zinc White and the Influence of Paint Composition for Stability in Oil Based Media". In: A. Burnstock, M. de Keijzer, J. Krueger, et al, editors. Issues in Contemporary Oil Paint. Cham, Switzerland: Springer International Publishing, 2014, pp.264–281.
24. J.J. Hermans, K. Keune, A. van Loon, et al. "The Molecular Structure of Three Types of Long-Chain Zinc(II) Alkanoates for the Study of Oil Paint Degradation". Polyhedron. 2014. 81: 335–340.
25. K.L.A. Chan, S.G. Kazarian. "Correcting the Effect of Refraction and Dispersion of Light in FT-IR Spectroscopic Imaging in Transmission through Thick Infrared Windows". Anal. Chem. 2013. 85: 1029–1036.
26. K.L.A. Chan, S.G. Kazarian. "Attenuated Total Reflection Fourier-Transform Infrared (ATR-FTIR) Imaging of Tissues and Live Cells". Chem. Soc. Rev. 2016. 45(7): 1850–1864.
27. V.A. Solé, E. Papillon, M. Cotte, et al. "A Multiplatform Code for the Analysis of Energy-Dispersive X-ray Fluorescence Spectra". Spectrochim. Acta, Part B. 2007. 62(1): 63–68.
28. F. Lacouture, J. Peultier, M. François, et al. "Anhydrous Polymeric Zinc(II) Octanoate". Acta Crystallogr. 2000. C56: 556–557.
29. C. Tamames-Tabar, E. Imbuluzqueta, N. Guillou, et al. "A Zn Azelate MOF: Combining Antibacterial Effect". CrystEngComm. 2015. 17: 456–462.
30. A. Mesbah, C. Juers, M. François, et al. "Structures of Magnesium and Zinc Long Aliphatic Chains Carboxylates". Z. Kristallogr. Suppl. 2007. 26: 593–598.
31. A. Mesbah, M. François. "Polymorphism and Polytypism in Zinc Aliphatic Carboxylate: The Complex Case of $Zn(C_{11}H_{21}O_2)_2$". Mater. Lett. 2017. 197: 228–232.
32. J. Catalano, A. Murphy, Y. Yao, et al. "Coordination Geometry of Lead Carboxylates – Spectroscopic and Crystallographic evidence". Dalton Trans. 2015. 44: 2340–2347.
33. F.J. Martínez-Casado, M. Ramos-Riesco, J.A. Rodríguez-Cheda, et al. "Lead(II) Soaps: Crystal Structures, Polymorphism, and Solid and Liquid Mesophases". Phys. Chem. Chem. Phys. 2017. 19(26): 17009–17018.
34. J. Hermans, K. Keune, A. van Loon, et al. "The Crystallization of Metal Soaps and Fatty Acids in Oil Paint Model Systems". Phys. Chem. Chem. Phys. 2016. 18: 10896–10905.
35. J. Economy, J. Mason, L. Wohrer. "Halatopolymers". J. Polym. Sci. A. 1970. 8: 2231–2244.
36. L. Baij, L. Chassouant, J.J. Hermans, et al. "The Concentration and Origins of Carboxylic Acid Groups in Oil Paint". RSC Adv. 2019. 9: 35559–35564.